Coupling of AC Grids via VSC-HVDC Interconnections for Oscillation Damping based on Differential and Common Power Control

Alberto Rodríguez-Cabero, Javier Roldán-Pérez, *Member, IEEE*, Milan Prodanovic, *Member, IEEE*, Jon Are Suul, *Member, IEEE*, and Salvatore D'Arco.

***Abstract*—This paper presents a control approach for HVDC interconnections that provides damping of frequency oscillations in asynchronous ac grids by introducing a virtual friction for coupling their inertial dynamics. The HVDC interconnection is modelled by using the concept of common and differential power flow, allowing for independent control of the dc voltage and the net power transfer between HVDC terminals, respectively. The proposed controller introduces a damping effect in the differential power flow which is equivalent to a mechanical friction between the generators connected to the ac grids at the two terminals. This virtual friction-based damping can effectively attenuate poorly damped frequency oscillations that can be observed where the HVDC interconnection is interfaced to either of the ac grids without relying on fast communication between the converter terminals. The impact of the proposed control technique on the stability and damping of two interconnected power systems is first analysed by using a simplified model. Then, the sensitivity to the frequency and damping of the oscillation modes appearing in the ac grid frequencies, as well as the effect of the dc line resistance on the oscillation damping are evaluated. Finally, the control system performance is experimentally validated on a scaled laboratory setup.**

I. Introduction

Low-frequency electro-mechanical oscillations in traditional power systems (i.e. intra-area and/or inter-area oscillations) are largely defined by the inertia and damping of the synchronous generators, their governors and excitation systems, and the power system topology [1]. Therefore, methods for Power Oscillation Damping (POD) and attenuation of frequency oscillations have been widely studied in traditional interconnected power systems. Since the early practical applications of power electronic technology in the transmission system, POD control has also been investigated for HVDC interconnections [2, 3]. Initial research efforts focused on POD by Current Source Converter (CSC) HVDC systems while HVDC links based on Voltage Source Converters (VSCs) have been increasingly preferred during the last decade [4]. Thus, recent research efforts have been mainly focused on the possibility offered by utilizing VSC-HVDC interconnections for improving power systems stability and contributing to damping of low frequency oscillations [5–8].

In modern power systems, Renewable Energy Sources (RES) with power electronic grid interfaces are increasingly replacing traditional generation plants [9]. However, power electronic converters with conventional control strategies do not inherently provide physical inertia, and reduced equivalent system inertia may compromise the stability of power systems under severe disturbances [10]. Therefore, new oscillatory issues related to the increasing penetration of power electronics converters are also becoming important [11].

To compensate for reduced equivalent system inertia, some authors have proposed specific control strategies for HVDC systems that emulate the dynamic properties of synchronous generators [12–14]. This is becoming an attractive control approach since power systems are inherently designed to operate with synchronous generators and, once their control parameters are properly set, such converters can contribute to the power system stabilisation. However, in most cases, this approach implies the dc-voltage regulation has to be in the same time-scale (or slower) than the synchronous machine dynamics, and this can threaten the dc-voltage stability.

Without considering contributions to the equivalent system inertia, several control strategies have also been proposed for utilizing HVDC-links to damp oscillations in emerging power system configurations. For example, Zeni *et al.* [6] recommended guidelines for controller design in order to damp oscillations in HVDC links connected to off-shore wind-farms. In [15] a supplementary controller based on neural networks was introduced for inter-area Power Oscillation Damping (POD). The method provides accurate results, but it is computationally intensive. Other authors focused on control strategies for POD by using Wide Area Measurement Signals (WAMS). For example, Preece *et al.* [16] demonstrated a controller for POD based on a Linear Quadratic Gaussian regulator by using WAMS. Pierre *et al.* [17] proposed a supervisory controller for inter-area POD by using real-time

Manuscript received April 25, 2019; revised August 2, 2019, and October 16, 2019; accepted October 31, 2019. The work of IMDEA Energy Institute received financial support from Community of Madrid, through the research project PROMINT-CM, Ref: P2018/EMT4366. The work of SINTEF Energy Research was supported by the project HVDC Inertia Provision (HVDC Pro), financed by the ENERGIX program of the Research Council of Norway (project number 268053/E20) and the industry partners; Statnett, Equinor, RTE and ELIA. (*Corresponding author: Alberto Rodríguez-Cabero*)

Alberto Rodríguez-Cabero, Milan Prodanovic and Javier Roldán-Pérez are with the Electrical Systems Unit, IMDEA Energy Institute, Madrid, 28935 Spain. (e-mail: alberto.rodriguez, milan.prodanovic, javier.roldan@imdea.org).

Jon Are Suul is with SINTEF Energy Research, 7465 Trondheim, Norway, and also with the Department of Engineering Cybernetics, Norwegian University of Science and Technology, 7491 Trondheim, Norway (e-mail: jon.a.suul@sintef.no).

Salvatore D'Arco is with SINTEF Energy Research, 7465 Trondheim, Norway (e-mail: salvatore.darco@sintef.no)

Color versions of one or more of the figures in this paper are available online at http://ieeexplore.ieee.org.

This article has been accepted for publication in a future issue of this journal, but has not been fully edited. Content may change prior to final publication. Citation information: DOI 10.1109/TPEL.2019.2952656, IEEE Transactions on Power Electronics

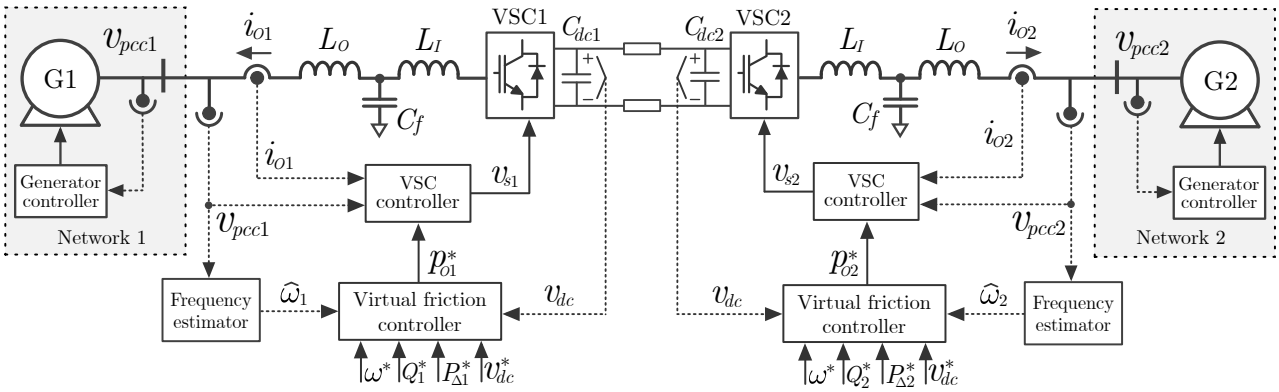

Fig. 1. Electrical and control diagram of a point-to-point HVDC connection providing virtual friction and voltage support to both sides.

frequency measurements, while Agnihotri *et al.* [18] designed a robust controller that considered partial and complete loss of communications. These control strategies showed satisfactory performance, but the requirement of fast communication increases the system complexity and reduces reliability [19].

To avoid dependency on high-bandwidth communication between HVDC terminals, control strategies that use the dc-link voltage as an indicator of the ac network frequency deviation have been proposed. One of the first attempts was introduced by Phulpin [20], who proposed a communication-free controller that allowed offshore wind generators connected via VSC-HVDC links to provide inertia to the mainland ac grid. Recently, some authors have proposed coordinated control strategies to provide frequency support and/or inertia emulation via coordinated dc-voltage regulation [11, 21, 22]. In particular, Rouzbehi *et al.* [23] introduced the concept of inertia sharing for ac systems coupled by MTDC links. The control scheme provided a virtual coupling between ac networks, increasing the equivalent system inertia. However, coupling of lightly-damped ac systems and damping of low frequency power oscillations was not addressed.

This paper introduces a controller for VSC-HVDC links that introduces virtual electro-mechanical friction between two power systems. As introduced in [24], the design of the proposed control strategy is based on equivalent swing equation models representing the interconnected power systems. Frequency support as well as damping of frequency oscillations at both sides of the HVDC link is inherently provided by the control strategy. The implementation uses the differential and common power concept introduced in [25]. This approach allows independent control of the dc voltage and the power transfer of the HVDC link, and it is demonstrated how this representation assigns physical meanings to the controller gains of the proposed virtual friction control.

Based on the general concepts introduced in [24], this paper addresses the controller implementation in detail, and shows that the proposed approach allows a straightforward implementation of the virtual friction control with no need of communication between the HVDC converter terminals. Furthermore, the POD capability of the proposed controller is analytically evaluated by using a simplified model of the two ac networks connected via the HVDC-link. The impact of the oscillation frequency and damping of the oscillations in the two grid frequencies is analysed in detail as well as the impact of the dc line resistance on the POD capability. Finally, the performance of the control scheme is experimentally validated by using a scaled prototype of the VSC-HVDC link.

II. System Overview and Modelling

A. Reference System Configuration

Fig. 1 shows the electrical and control system diagram of the point-to-point VSC-HVDC configuration considered in this paper, consisting of two VSC terminals (VSC1 and VSC2) that interconnect two asynchronous grids. For analysing the operation of the VSC terminals for damping low frequency power system oscillations, the two different asynchronous areas can be modelled as equivalent generators that aggregate the electro-mechanical dynamics of each area [1]. Therefore, the dynamics of the ac networks considered in this paper are represented by two equivalent generators (G1 and G2).

The control of the two VSCs terminals include traditional inner loop controllers and they are operate as power-controlled sources that inject or absorb active and reactive powers from the ac grids. For each terminal, the grid-side current, the output voltage and dc-capacitor voltage are denoted as i_o, v_s and v_{dc}, respectively. The two terminals (1 and 2) are indicated as variable subscripts (i.e. i_{o1}). The dc capacitor of each VSC is referred as C_{dc}, and the total equivalent capacitance of the dc system is given by $C'_{dc} = C_{dc1} + C_{dc2} + C_{cable}$, where C_{cable} is the equivalent capacitance of the dc cable interconnecting the VSC terminals.

Both terminals are assumed to have identical controllers with an inner power controller ('VSC controller') cascaded with an outer loop controller ('Virtual friction controller') that emulates the effect of a friction between the two equivalent generators and regulates the dc-link voltage.

B. Equivalent Generator Modelling

The linearised swing equation of generator G1 can be written as follows (and the same equation can be used for generator G2) [26, 27]:

$$2H_1 \frac{d\Delta\omega_1}{dt} = \Delta P_{m1} - \Delta P_{e1} - D_1 \Delta\omega_1, \qquad (1)$$

where "Δ" is the incremental operator, H_1 is the equivalent inertia constant of the synchronous area, D_1 is the equivalent

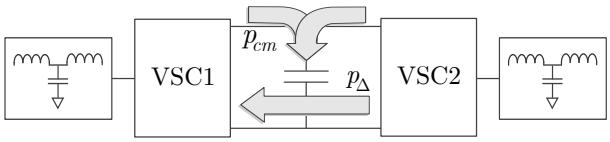

Fig. 2. Power flow representation in a Back to Back configuration based on the common and differential power concepts.

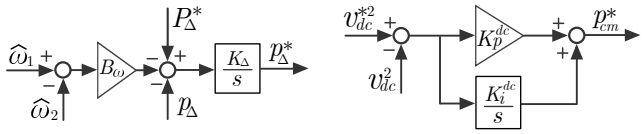

(a) (b)

Fig. 3. Block diagram of (a) a differential power controller emulating the effect of a mechanical friction, and (b) the dc-voltage controller based on the common power concept. Centralised implementation [29].

damping factor of the area, ω_1 is the area angular frequency, P_{m1} is the mechanical power supplied by the equivalent turbine, and P_{e1} is the electrical power demanded by the local area load [1]. The mechanical power P_{m1} is controlled by using an equivalent turbine speed governor represented as a first-order low-pass-filter [1], where R_1 is the frequency droop coefficient, and T_1 is a time constant that models the delayed response of the turbine actuator [26]. Thus, the dynamic equation of the governor in Laplace domain is:

$$\Delta P_{m1} = \Delta P^* + R_1/(T_1 s + 1) \cdot (\Delta\omega^* - \Delta\omega_1), \quad (2)$$

where P^* and ω^* are the active power and angular frequency set points, respectively. For the sake of simplicity, the incremental operator "Δ" will be omitted in the rest of the paper.

The applied model is the simplest representation of the dynamics of a synchronous generator, modelled as a second-order system. Thus, this model provides an easy interpretation of the coupling effect introduced by the proposed control system and it will be used to represent the frequency oscillations that can be measured at the HVDC terminals. A similar approach for simplified representation of ac grids has been recently justified in [28], for analysis of the performance of HVDC links in damping of inter-area oscillations. Thus, any intra-area or inter-area oscillations that can be detected in the frequency estimated at the HVDC terminals can be equivalently represented by a second-order system. It is important to remark that the proposed control concept is generic and it can be applied in any arbitrary complex power network model. However, a simplified equivalent model of each ac grid is convenient for demonstration and analytical evaluation of the virtual friction concept, while analysis of the influence from the detailed power system configuration on the dynamic performances of the proposed control strategy is considered as a further research.

C. Common and Differential Power Concepts

The concept of differential and common power was introduced in [25] with Fig. 2 showing an example of its application to a Back-to-Back (BTB) configuration. The active power flow can be defined by:

$$p_{cm} = -(p_{o1} + p_{o2}), \quad (3)$$

$$p_\Delta = (p_{o1} - p_{o2})/2, \quad (4)$$

where p_{o1} and p_{o2} are the instantaneous active powers delivered to the ac grids by VSC1 and VSC2, respectively while p_{cm} and p_Δ represent the common and differential powers. The main advantage of this representation is the decoupling of the active power flow determining the dc link voltage dynamics, associated with p_{cm}, from the net active power flowing from G2 to G1, associated to p_Δ [25]. The proposed controller takes advantage of this property to provide:

- A fast and accurate control of the dc-link voltage by controlling the common-mode power p_{cm}.
- An effect similar to that of a mechanical friction between the two generators by controlling differential power p_Δ.

The output powers p_{o1} and p_{o2} can be expressed as a function of the differential and common power, (3) and (4), yielding:

$$p_{o1} = p_\Delta - p_{cm}/2, \quad (5)$$

$$p_{o2} = -p_\Delta - p_{cm}/2. \quad (6)$$

These expressions will be used later to calculate the power references for each VSC as a function of their common and differential power references.

III. Introduction to the Virtual Friction Concept

A. Differential Power and its Equivalent Mechanical Effect

The differential power p_Δ is associated to the active power exchange between grids, if losses and energy stored in the *LCL* filters of the terminals are neglected. As first introduced in [29], the differential power can be controlled to provide an effect equivalent to that of a mechanical friction between the ac networks. With this aim, the following expression is defined:

$$p^*_\Delta = (K_\Delta/s) \cdot (P^*_\Delta - p_\Delta + B_\omega(\hat{\omega}_1 - \hat{\omega}_2)). \quad (7)$$

The hat "$\hat{}$" refers to estimated values, p^*_Δ is the differential power reference for the inner controller, P^*_Δ is the differential power set point, K_Δ is the integral gain, and B_ω is the equivalent mechanical friction to be inserted between the electrical grids that will be explained in the following. Fig. 3 (a) shows the block diagram of a centralised controller based on this concept [29].

If the transient response of the differential-power controller is significantly faster than that of the equivalent generators (G1 and G2), its dynamics can be neglected for system-level studies. This assumption will be guaranteed during the design process. Thus, the differential power can be expressed as:

$$p_\Delta = P^*_\Delta + B_\omega(\hat{\omega}_1 - \hat{\omega}_2). \quad (8)$$

Moreover, if power losses are neglected, the swing equations of both equivalent generators can be expressed in terms of the HVDC terminals active powers, $p_{e1} = -p_{o1}$ and $p_{e2} = -p_{o2}$. Therefore, by substituting (5) and (6) in (1) (and the same equation for G2):

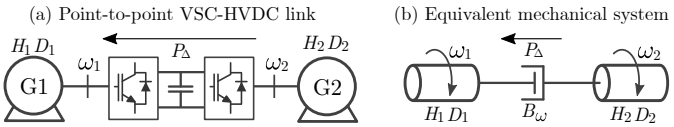

Fig. 4. (a) Electrical diagram of a point-to-point link. (b) Equivalent mechanical diagram of the point-to-point link with the virtual friction controller.

$$2H_1\frac{d\omega_1}{dt} = P_{m1} + P^*_\Delta + B_\omega(\hat{\omega}_1 - \hat{\omega}_2) - p_{cm}/2 - D_1\omega_1, \quad (9)$$

$$2H_2\frac{d\omega_2}{dt} = P_{m2} - P^*_\Delta - B_\omega(\hat{\omega}_1 - \hat{\omega}_2) - p_{cm}/2 - D_2\omega_2. \quad (10)$$

In (9) and (10), the coefficient B_ω multiplies the difference of the two generator speeds and its effect is equivalent to that of a mechanical friction inserted between G1 and G2. The differential power reference P^*_Δ represents the power exchanged between the shafts, while the common power p_{cm} represents the power that flows into the dc capacitor. Fig. 4 represents this concept, graphically.

B. Common Power Based dc-Voltage Controller

By neglecting losses and energy stored in the elements of *LCL* filters, the dynamic equation that models the energy stored in the dc capacitance can be written as [25]:

$$C'_{dc}/2 \cdot dv^2_{dc}/dt = p_{cm}. \quad (11)$$

Since the common power p_{cm} is directly related to the energy stored in the dc capacitance, the dc voltage can be regulated by controlling the common-power with a PI controller as shown in Fig. 3 (b).

IV. Implementation of the Controller without Communications between Terminals

In Section III, it has been assumed that measurements from both terminals are available to a common controller. However, as already mentioned, it will be preferable to avoid dependency on high bandwidth communication between the terminals of a HVDC interconnection. As shown in the following, a decentralised control scheme can be developed, where only measurements from a single terminal are assumed available to each controller. An overview of the resulting implementation of the virtual friction controller for terminal 1 is shown in Fig. 5. The same scheme (with the notation adapted) is used for terminal 2.

A. Implementation of the Equivalent Mechanical Friction

In order to implement a decentralized control scheme, two new variables, $\tilde{p}^*_{\Delta 1}$ and $\tilde{p}^*_{\Delta 2}$, are defined. For the terminal 1, its new variable is:

$$\tilde{p}^*_{\Delta 1} = (K_\Delta/s)\cdot(P^*_{\Delta 1} - p_{o1} + 2B_\omega(\omega^* - \hat{\omega}_1) - D_{dc}(v^{*2}_{dc} - v^2_{dc})), \quad (12)$$

where D_{dc} is a droop coefficient for the dc-voltage that has been added to the original expression of p^*_Δ in (7). Its main objective is to share information between terminals regarding mismatches in $\tilde{p}^*_{\Delta 1}$ and $\tilde{p}^*_{\Delta 2}$.

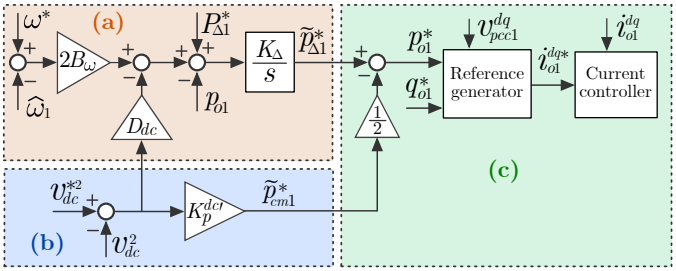

Fig. 5. Block diagram of the implemented dc-voltage and virtual friction controllers for terminal 1: (a) Differential power and virtual friction controller, (b) dc-voltage controller and (c) current controller and reference generator.

Following the same procedure presented in Section III-A, the steady state values for the decentralised implementation can be calculated. In steady state, if (12) and the equivalent version of the same equation for terminal 2 are subtracted and divided by two, the following relationship is obtained:

$$\underbrace{(p_{o1} - p_{o2})/2}_{p_\Delta} = \underbrace{(P^*_{\Delta 1} - P^*_{\Delta 2})/2}_{p^*_\Delta} + B_\omega(\hat{\omega}_1 - \hat{\omega}_2) = 0. \quad (13)$$

If the droop coefficients of both VSCs have the same value, steady-state equation (13) is similar to steady-state equation (7). Repeating the same procedure introduced in Section III-A, it can be demonstrated that the effect of the frequency droop B_ω is again equivalent to a virtual friction inserted between the two generators (see Fig. 4). The block diagram of the proposed controller for terminal 1 is shown in Fig. 5 (a).

B. Implementation of the dc-Voltage Controller

Since both VSCs share the control of the dc-voltage, the use of two integral actions should be avoided [30]. Therefore, a P controller has been used:

$$\tilde{p}^*_{cm1} = K_p^{dc'} \cdot (v^{*2}_{dc} - v^2_{dc}). \quad (14)$$

where $K_p^{dc'}$ is the dc controller gain.

C. Reactive Power Controller

Reactive power injection at each terminal can be controlled independently:

$$q^*_o = (K_Q/s)\cdot(Q^*_o - q_o + D_V(|\vec{v}^*_{pcc}| - |\vec{v}_{pcc}|)), \quad (15)$$

where Q^*_o is the reactive power set point, q_o is the instantaneous value of the reactive power, D_V is the reactive power-voltage droop coefficient, and $|\vec{v}^*_{pcc}|$ and $|\vec{v}_{pcc}|$ are the module of the PCC voltage space vector and its reference value, respectively.

D. Power Reference Generation

Fig. 5 (c) shows the block diagram of the power reference generator. The proposed controller will generate the reference values for p_Δ and p_{cm} (p^*_Δ and p^*_{cm}, respectively). Active power references (p^*_{o1} and p^*_{o2}) are obtained by manipulating

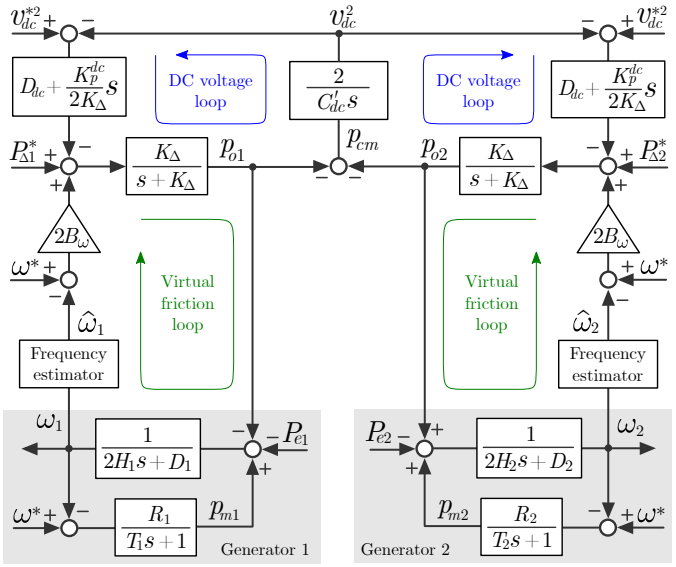

Fig. 6. Equivalent block diagram of two generators connected via a HVDC link with the proposed controller applied.

the differential and common power expressions, (3) and (4), yielding:

$$p^*_{o1} = \tilde{p}^*_{\Delta 1} - \tilde{p}^*_{cm1}/2, \tag{16}$$

$$p^*_{o2} = \tilde{p}^*_{\Delta 2} - \tilde{p}^*_{cm2}/2. \tag{17}$$

Reactive power references can be set independently (q^*_{o1} and q^*_{o2}). Current references are generated by using the output power of each terminal, independently. Therefore, for one terminal, the dq-axes current references can be written as [31]:

$$i^{d*}_o = p^*_o/v^d_{pcc}, \quad i^{q*}_o = -q^*_o/v^d_{pcc}. \tag{18}$$

V. Control Parameters Design

A. Equivalent Control System

Fig. 6 shows the equivalent block diagram of two generators connected via a HVDC interconnection with the proposed controller applied. The frequency estimator used in this paper can be found in [32]. This equivalent diagram can be derived from the block diagram depicted in Fig. 5, and adding the synchronous generators models. First, if the transient response of the current controller is faster than that of the dc-voltage and virtual friction controllers, the dynamics of the current controller can be neglected. Therefore, $p^*_{o1} \approx p_{o1}$. Second, the integral action that gives $\tilde{p}^*_\Delta$ is moved to the power command p_{o1} and a derivative is added to the common power loop $\hat{p}^*_{cm}$. After these manipulations, it can be seen that the common-mode dc-link controller is equivalent to a proportional-derivative controller, yet without an explicit derivative action.

B. Active and Reactive Controllers Design

In order to avoid interactions between the current, dc-voltage and virtual friction controllers, their time constants should be sufficiently separated [33]. If this condition is met, the input-output transfer function of the active power controller for the VSC1 can be written as:

$$\frac{P_{o1}(s)}{P^*_{\Delta 1}(s)} = \frac{K_\Delta}{s + K_\Delta}. \tag{19}$$

Following a similar approach for the reactive power controller:

$$\frac{Q_{o1}(s)}{Q^*_{o1}(s)} = \frac{K_{Q1}}{s + K_{Q1}}. \tag{20}$$

Therefore, the frequency of the closed-loop poles can be selected by using $K_\Delta = \omega_p$ and $K_{Q1} = \omega_{Q1}$.

C. DC Voltage Controllers Design

The dc voltage controller is designed as a P controller where the frequency of the first-order closed-loop system can be selected by using the expression:

$$K^{dc'}_p = \omega_p C'_{dc}. \tag{21}$$

D. DC-Voltage Droop Design

The steady-state equation of the virtual friction controller in (12) can be written as (one for each VSC):

$$P^*_{\Delta 1} - p_{o1} + 2B_\omega(\omega^* - \hat{\omega}_1) - D_{dc}(v^{*2}_{dc} - v^2_{dc}) = 0, \tag{22}$$

By adding (22) and the equivalent expression derived for the VSC2, a new steady-state equation that relates the dc-voltage and the ac-frequency deviations is obtained:

$$\begin{aligned}(P^*_{\Delta 1} + P^*_{\Delta 2}) - (p_{o1} + p_{o2}) + 4B_\omega(\omega^* - \overline{\omega}_{12}) + \\ -2D_{dc}(v^{*2}_{dc} - v^2_{dc}) = 0.\end{aligned} \tag{23}$$

where $\overline{\omega}_{12}$ is the mean of the two ac grid frequencies, and it is calculated as follows:

$$\overline{\omega}_{12} = (\hat{\omega}_1 + \hat{\omega}_2)/2. \tag{24}$$

Assuming that the system operates in steady-state, the power consumed by the link are the losses: $p_{o1} + p_{o2} \approx -p_{loss}$. Additionally, in (12), the same power reference has to be used for both terminals: $P^*_{\Delta 1} = -P^*_{\Delta 2} = P^*_\Delta$, and the dc-voltage controllers have the same value ($K^{dc'}_p$). Under these considerations, the power balance equation in (23) becomes:

$$4B_\omega(\omega^* - \overline{\omega}_{12}) + p_{loss} = 2D_{dc}(v^{*2}_{dc} - v^2_{dc}). \tag{25}$$

This relationship can be used to design the dc-voltage droop gain (D_{dc}). By using (25) and according to the maximum dc-voltage deviation ($v_{dc} = v^*_{dc} \pm \Delta V_{dc}$), the dc-voltage droop gain can be calculated as:

$$D_{dc} = \frac{4B_\omega(\omega^* - \overline{\omega}_{12}) + \hat{p}_{loss}}{2(v^{*2}_{dc} - v^2_{dc})}. \tag{26}$$

where $\hat{p}_{loss}$ are the estimated power losses dissipated in the HVDC interconnection. However, the power losses are not constant and can vary depending on the operating conditions. One should note that D_{dc} is selected to establish a steady-state relation between dc voltage and ac frequencies. Its value is not critical for the system stability within a reasonable range and it can be chosen according to the requirements for droop settings.

This article has been accepted for publication in a future issue of this journal, but has not been fully edited. Content may change prior to final publication. Citation information: DOI 10.1109/TPEL.2019.2952656, IEEE Transactions on Power Electronics

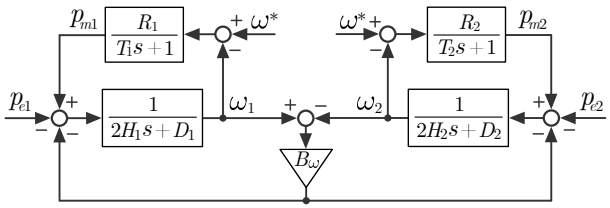

Fig. 7. Simplified block diagram of the two power networks connected via the virtual friction.

TABLE I
PARAMETERS OF THE EQUIVALENT GENERATORS

Var.	Value	Var.	Value
H_1	1/5 pu	H_2	1/200 pu
D_1	0	D_2	0
R_1	0.5	R_2	0.5
T_1	0.5 s	T_2	3 s
ζ_1	0.63	ζ_2	0.04
ω_{os1}	1.58 rad/s	ω_{os2}	4.08 rad/s

VI. Analytical Results

This section presents results from an analytical evaluation of the impact from the proposed controller on a simplified model of the two networks interconnected. This simplified model can be derived from the block diagram depicted in Fig. 6. If the dynamics of the dc capacitor and power controllers are significantly faster than the generator dynamics, they can be neglected and the block diagram can be simplified to Fig. 7.

A. Analysis of the Virtual Friction Concept

The impact of virtual friction gain B_ω on the oscillations of the equivalent generators G1 and G2 is analysed in this section. The parameters of the equivalent generators can be found in Table I. According to these parameters, generator G1 has a damping factor of $\zeta_1 = 0.63$, while generator G2 has a damping factor of $\zeta_2 = 0.04$ (low damping). When the two systems are not coupled via the HVDC link, ω_{os1} and ω_{os2} are the natural frequencies of G1 and G2 respectively. Fig. 8 (a) and (b) show the trajectories of the closed loop poles of the transfer functions $\omega_1(s)/P_{e1}(s)$ and $\omega_2(s)/P_{e2}(s)$ when B_ω varies. For $B_\omega = 0$ (green poles), the two networks are

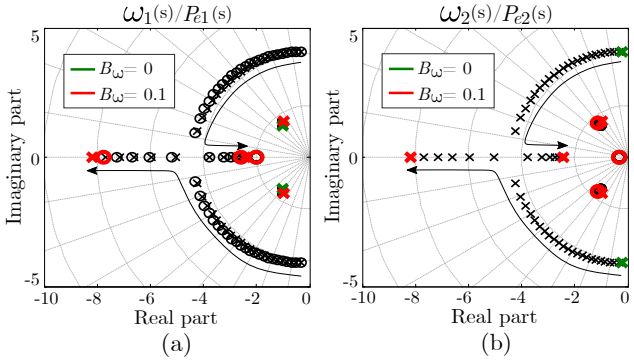

Fig. 8. Pole trajectories of the transfer functions (a) $\omega_1(s)/P_{e1}(s)$ and (b) $\omega_2(s)/P_{e2}(s)$ for different virtual friction values.

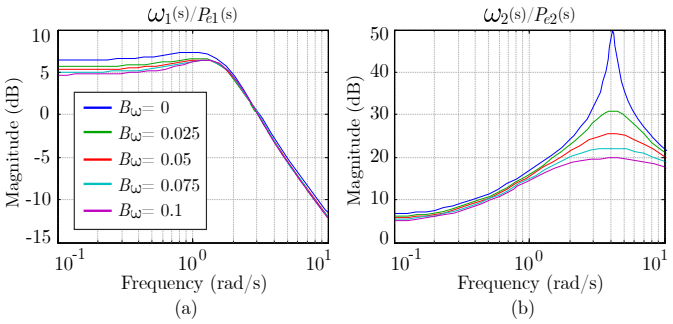

Fig. 9. Bode plot of the transfer functions (a) $\omega_1(s)/P_{e1}(s)$ and (b) $\omega_2(s)/P_{e2}(s)$ for different virtual friction values.

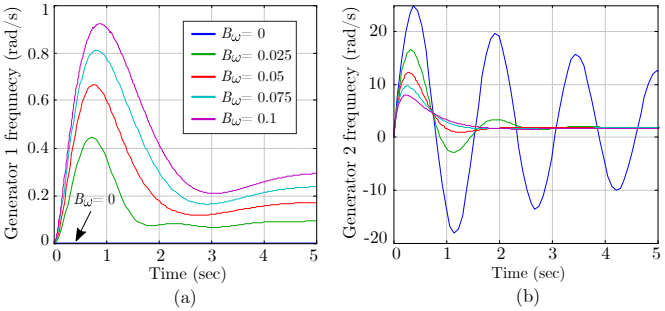

Fig. 10. Simulation results: Transient response of two power networks interconnected via a virtual friction when a step-change was applied to G2 active power. (a) Angular frequency of G1 (ω_1), and (b) angular frequency of G2 (ω_2).

decoupled and the transfer functions exhibit different poles. Generator 1 presents two complex poles that have frequency of 1.58 rad/s and damping factor of 0.632, while generator 2 presents two complex poles that have frequency of 4.08 rad/s and damping factor of 0.04. When B_ω increases, the complex poles of G2 move away from the stability limit, increasing their damping factor until they reach the real axis and become real. For $B_\omega = 0.1$ (red poles), one of the real poles moves towards the stability limit, reducing its frequency, while the other moves away increasing its frequency. The poles of G1 are almost not affected by the variation of B_ω.

Fig. 9 (a) and (b) show the bode plot of the transfer functions $\omega_1(s)/P_{e1}(s)$ and $\omega_2(s)/P_{e2}(s)$ for different values of B_ω. For $B_\omega = 0$ (blue line), both networks are fully decoupled and G2 exhibits a resonance peak. The virtual friction value introduces a coupling term and allows a power exchange between the two networks. It can be seen that increasing B_ω reduces the resonance peak at G2.

Fig. 10 shows the transient response of two networks connected by using a virtual friction when a step-change was applied to the active power demanded by network 2 P_{e2} for different values of B_ω. For $B_\omega = 0$ (blue lines), the two networks are decoupled and step change excited the low-frequency resonance of G2, producing a poorly damped frequency oscillation (Fig. 10 (b)). For $B_\omega > 0$, the two networks are coupled by the virtual friction and the impact of the disturbance can be mitigated. When B_ω increases, the coupling effect increases and network 1 supports network 2 when a disturbance takes place, effectively damping the frequency oscillation.

This article has been accepted for publication in a future issue of this journal, but has not been fully edited. Content may change prior to final publication. Citation information: DOI 10.1109/TPEL.2019.2952656, IEEE Transactions on Power Electronics

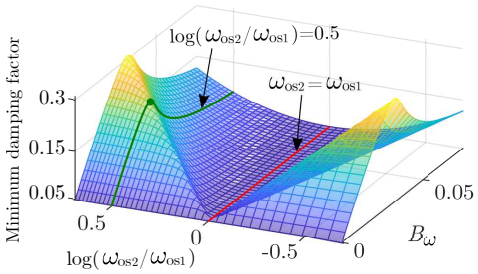

(a) G1 damping factor $\zeta_1 = 0.05$

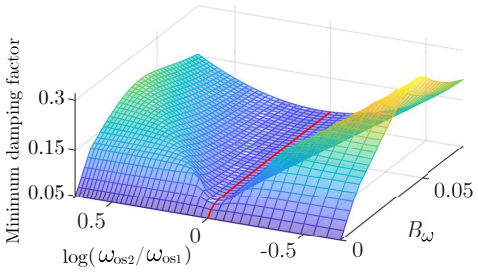

(b) G1 damping factor $\zeta_1 = 0.1$

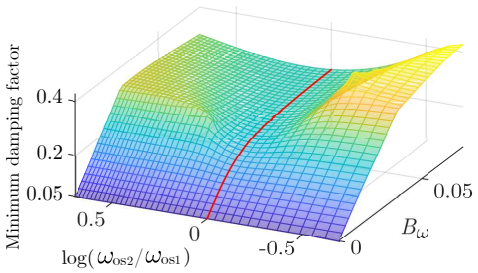

(c) G1 damping factor $\zeta_1 = 0.3$

Fig. 11. Minimum damping factors of the poles of the simplified model, when the oscillation frequency ratio $(\omega_{os2}/\omega_{os1})$ and B_ω vary.

B. Impact of Area Modes on the Damping Capability

In this section, the impact of the oscillation frequency of G1 and G2 on the POD capability of the controller is investigated. The parameters of G2 were maintained constant and they were chosen so that G2 has a poorly damped oscillation mode: $\zeta_2 = 0.05$ and $\omega_{os2} = 2$ rad/s. The parameters of G1 were selected in order to vary its oscillation frequency (ω_{os1}) between $\omega_{os2}/2$ and $2\omega_{os2}$. Three different values for the damping factor were considered: $\zeta_1 = 0.05$, $\zeta_1 = 0.1$ and $\zeta_1 = 0.3$. Fig. 11 shows the minimum damping factors obtained among all the poles of the simplified model. The logarithm of the ratio between area oscillation frequencies $(\omega_{os2}/\omega_{os1})$ is used in one axis, while the virtual friction (B_ω) in the other. The logarithm was chosen in order to improve the figure visualisation. Fig. 11(a) shows the case in which $\zeta_1 = 0.05$ (both generators have low damping factors). For $B_\omega = 0$, the minimum damping factor is 0.05 and, as B_ω increases, the minimum damping factor also increases until the maximum damping is achieved. Further increase of B_ω leads to a slight decrease of the minimum damping factor. It can be seen that the damping effect introduced by changing B_ω is less pronounced when the oscillation frequencies are similar $(\omega_{os2}/\omega_{os1} \approx 1)$. Particularly, when $\omega_{os2} = \omega_{os1}$ (marked with a red line), the minimum damping factor remains constant regardless the value of B_ω.

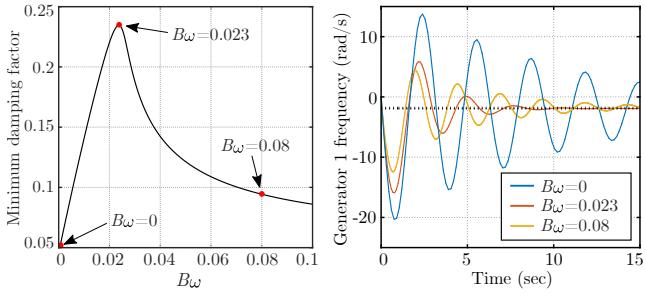

Fig. 12. (a) Minimum damping factor for $\omega_{os2} = 2$ rad/s and $\omega_{os1} = 3.29$ rad/s, when B_ω varies. (b) Transient response of G2 frequency (ω_2) for a step change in the load of G2.

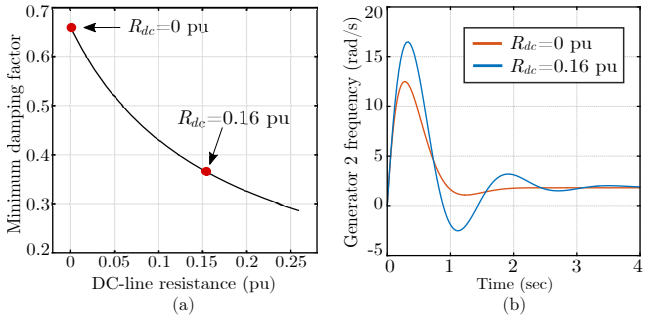

Fig. 13. Impact of the dc-line resistance: (a) Minimum damping factor when the dc-line resistor increases. (b) Transient response of simulation model including and excluding dc-line resistance of $R_{dc} = 0.16$ pu.

Fig. 11(b) and (c) show the minimum damping for $\zeta_1 = 0.1$ and $\zeta_1 = 0.3$, respectively. As in case (a), when B_ω increases, the minimum damping factor also increases until the maximum damping is achieved. It is worth noting that the damping effect introduced by B_ω is less effective when oscillation frequencies are similar. However, this becomes less significant when the damping factor of either generator is sufficiently large (see Fig. 11(c)).

A similar analysis was performed for the particular case of $\log(\omega_{os2}/\omega_{os1}) = 0.5$ ($\omega_{os2} = 2$ rad/s and $\omega_{os1} = 3.29$ rad/s), and damping factors of $\zeta_1 = 0.05$ and $\zeta_2 = 0.05$. Fig. 12(a) shows the minimum damping factor obtained when B_ω varies. It can be seen that the minimum damping factor has a maximum value for $B_\omega = 0.023$. Fig. 12(b) shows the transient response of the simulation model for different values of B_ω. For $B_\omega > 0$ the transient response is more damped. Moreover, for $B_\omega = 0.023$, the transient response is slightly more damped than for $B_\omega = 0.08$.

These results demonstrate that the proposed controller can increase the minimum damping factor of the system even when both generators have similar sizes and low damping factors. However, the damping effect is less effective when the oscillation frequencies are close to each other and the damping factors are low. As the difference between the oscillation frequencies and/or or the damping in one of the grids increases, the POD capability increases. These results are consistent with previous research studies that highlighted the impact of the ratio between modal frequencies on the POD capability between two asynchronous networks [28].

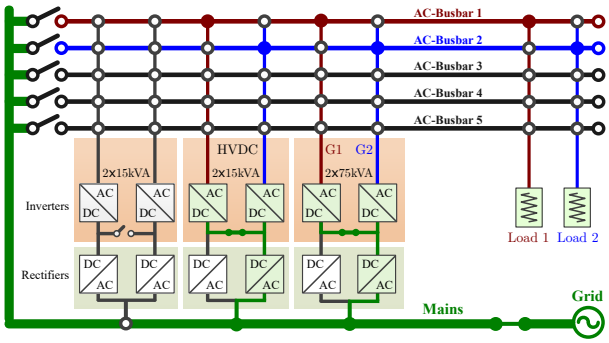

Fig. 14. Electric diagram of the Smart Energy Integration Lab (SEIL).

C. Impact of the dc Line on the POD Capability

The impact of the dc-line resistance was evaluated analytically and in simulation. The parameters of the equivalent generators can be found in Table I. Fig. 13 (a) shows the minimum damping factor when a dc line resistance (R_{dc}) is included in the small-signal model of the complete system. Meanwhile, Fig.13 (b) shows the transient response of the detailed simulation (grey) excluding and (black) including the dc resistance, for $R_{dc} = 0.16$ pu. The line resistance decreases the damping provided by the controller. However, typical values of dc-line resistances are smaller than the values considered here. Therefore, the POD capability of the controller would not be compromised.

VII. Experimental Results

A. Description of the experimental setup

The proposed virtual friction control system has been experimentally validated in the Smart Energy Integration Lab (SEIL) [34], by a scaled version of the power system depicted in Fig. 1. Fig. 14 shows a schematic diagram of the laboratory facilities. The nominal grid voltage and frequency of both ac grids is 400 V and 50 Hz. The ac grids represented in this paper by the equivalent generators G1 and G2, are emulated by using two 75 kVA VSC with LCL filter (S_B=75 kVA) operated in closed-loop. A fourth order synchronous generator model is assumed which includes the mechanical shaft, the speed governor and the exciter to control the rotor field. The equivalent inductance of the synchronous generator is emulated by using the output filter of the VSC. Two 15 kVA converters in BTB configuration are used as the VSC-HVDC interconnection. The output filters are $L_I = 2.3$ mH, $C_f = 8.8$ μF and $L_o = 0.93$ mH, and the total dc-capacitance is $C'_{dc} = 1.2$ mF. The control systems is implemented on an embedded controller [34]. The sampling and switching frequencies of the 15 kVA BTB converters are 10 kHz while for the 75 kVA VSCs are 8 kHz.

B. Control System Specifications

The control parameters have been designed according to the procedure described in Section V. Conventional PI controllers designed to achieve a setting of $t_{set} < 4$ ms and an overshoot of $M_p < 15\%$ are used for the current controllers. The dc-voltage controller is designed to have a slower transient response than the current controllers with $\omega_p = 300$ rad/s. The active and reactive power controllers are designed to be even slower transient responses than the dc-voltage controller, $\omega_p = 2\pi 10$ rad/s and $\omega_{Q1} = \omega_{Q2} = 2\pi 10$ rad/s. The reactive power-voltage droop coefficients are determined by the application requirements. It this case, both VSCs have the same droop values $D_V = 0.01$ pu. The dc-voltage droop coefficient (D_{dc}) can the adjusted to achieve the desired steady-state relation between the frequency and dc-voltage deviations. In this case, it has been designed to achieve a dc-voltage deviation of 20 V for frequency deviation of 0.05 Hz. Also, the power losses of the HVDC link are estimated to be $\hat{p}_{loss} = 1$ kW. By using (26), the dc-voltage droop coefficient is set to $D_{dc} = 0.1$.

C. Oscillation Damping of a Poorly Damped Generator

In this section, the proposed controller was tested in a scenario where G1 presents well-damped transient response while G2 is characterized by a poorly damped oscillation mode. The parameters of generators can be found in Table I. By using these parameters, it is possible to compute the minimum damping factor of the system as a function of B_ω, similarly to Fig. 12(a). Then, the virtual friction value is selected to maximise the minimum damping factor of the system. In this case, the virtual friction was set to $B_\omega = 0.05$.

1) Oscillating Generator 2: Fig. 15(a) shows the transient response of the system when a step change of differential power reference P^*_Δ is applied, and the virtual friction is disabled. The differential power rapidly reaches the reference value and the frequency of G1 shows a well-damped response. However, when the active power changes, the low-frequency resonance is excited and the frequency of G2 exhibits a poorly damped oscillation. Fig. 15(c) shows the transient response of the system when a local load is connected to G2 (P_{e2}), and the virtual friction is disabled. In this case, when the load is connected, the low-frequency resonance is excited and the frequency of G2 exhibits again a poorly damped oscillation. These results are consistent with the analysis presented in Section VI.

2) Damping of Oscillations: Fig. 15(b) shows the transient response of the system when the virtual friction controller is included ($B_\omega = 0.05$) and a step-change of P^*_Δ is applied. In this case, the proposed controller is used to couple the two generators by using the virtual friction and allows an active power exchange between the generators depending on the difference of frequencies $\omega_1 - \omega_2$. Initially, the differential power shows a fast transient response, leading to a transient at the ac grid frequencies. Then, the differential power exhibits a transient response depending on the frequency dynamics of ac grids, and the control prevents excitation of the low-frequency resonance. Moreover, the dc voltage acts as a communication link between both terminals, indicating the need of active power support. Fig. 15(d) shows the transient response of the system when a local load is connected to G2 (P_{e2}), and the virtual friction is included ($B_\omega = 0.05$). When the load is connected, the low-frequency resonance is excited and the frequency of G2 deviates. The differential power shows a transient response proportional to the difference of

This article has been accepted for publication in a future issue of this journal, but has not been fully edited. Content may change prior to final publication. Citation information: DOI 10.1109/TPEL.2019.2952656, IEEE Transactions on Power Electronics

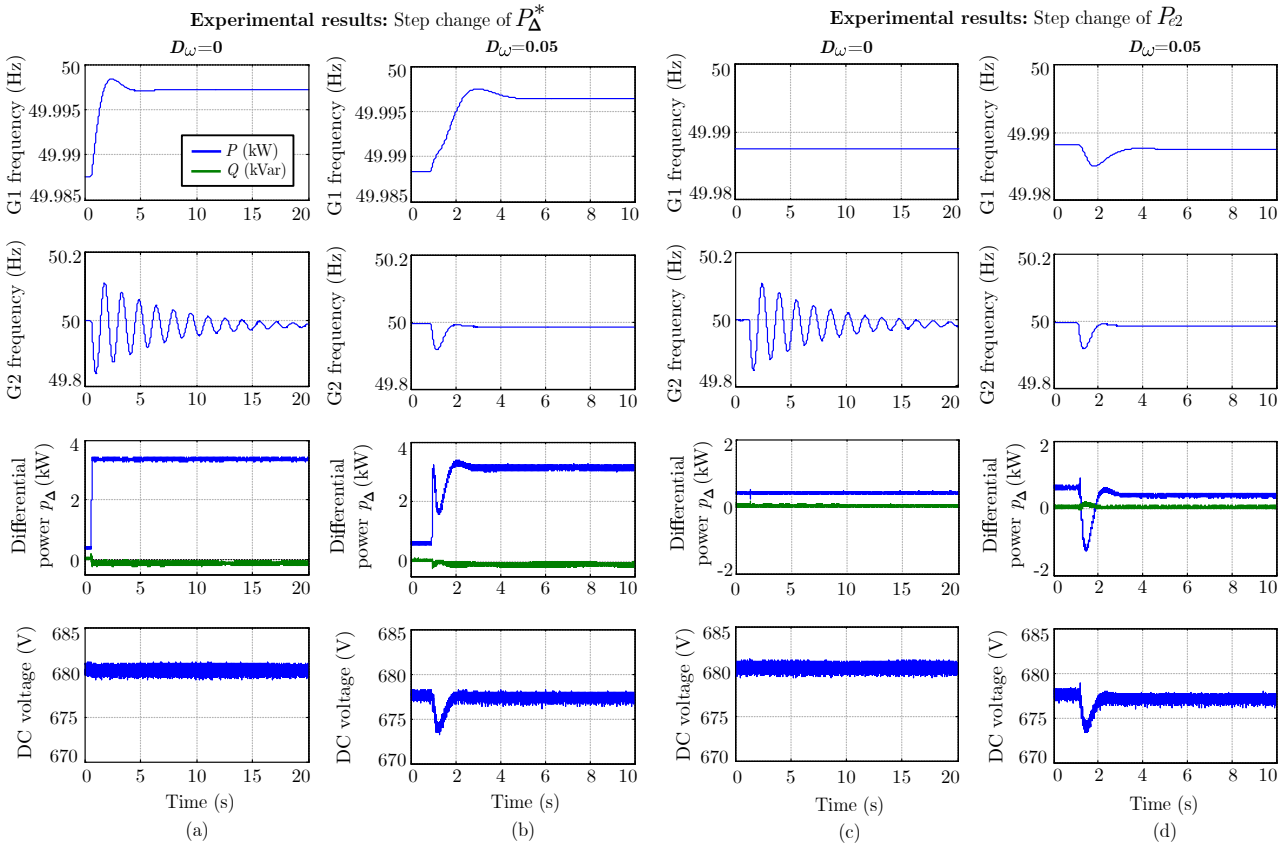

Fig. 15. Experimental results: Transient response of the system when: (a) Virtual friction is $B_\omega = 0$ pu and step-change of p^*_Δ is applied. (b) Virtual friction is $B_\omega = 0.05$ pu and step-change of p^*_Δ is applied. (c) Virtual friction is $B_\omega = 0$ pu and step-change of the local load of G2 (P_{e2}) is applied. (d) Virtual friction is $B_\omega = 0.05$ pu and step-change of the local load of G2 (P_{e2}) is applied.

frequencies, allowing the active power to flow from G1 to G2 and, more importantly, to damp the low-frequency oscillation. In both cases, the dc voltage shows transient responses depending on the frequency dynamics of the ac grids, acting as a communication link between both terminals and indicating the need of active power support. These results demonstrate that the proposed control provides a feature equivalent to a mechanical friction between the two generators, damping the frequency oscillations according to the designed virtual friction value. Also, the transient responses of both frequencies present a good match with the theoretical responses provided in Section VI-A, demonstrating the electro-mechanical coupling established between the two generators.

D. Oscillation Damping of Two Poorly Damped Generators

In this section, the proposed controller was tested in a scenario where both generators exhibit poorly damped oscillation modes. In this case, the damping factor of the generators was set to $\zeta_1 = \zeta_2 = 0.05$, while the oscillation frequency ratio varied. Fig. 16(a) shows the transient response of the system when a local load is connected to G1 and the oscillation frequency ratio is $\omega_{os2}/\omega_{o1} = 1$. When the virtual friction is disabled ($B_\omega = 0$), G1 exhibits the low frequency resonance while the G2 frequency remains constant. When the virtual friction is enabled ($B_\omega = 0.05$ and $B_\omega = 0.09$), both generators shared the disturbance featuring the same oscillation frequency. These results demonstrate that the proposed controller cannot provide effective POD when the equivalent generators of two poorly damped grids have the same oscillation frequency. This result is consistent with the analysis presented in Section VI-B.

Fig. 16(b) shows the transient response of the system when a local load is connected to G1 and the oscillation frequency ratio is $\omega_{os2}/\omega_{o1} = 1.64$. Unlike the previous case, when the virtual friction is enabled and $B_\omega > 0$, the proposed controller provides additional damping and the minimum damping of the system increase. When $B_\omega = 0.023$, the transient response exhibits the most damped response, while for $B_\omega = 0.09$ the transient response exhibits a less damped response. These results are consistent with the analysis presented in Section VI-B.

Fig. 16(c) shows the transient response of the system when the same disturbance is applied and $\omega_{os2}/\omega_{o1} = 2.71$. It can be seen that the damping effect introduced by the virtual friction B_ω increases as the oscillation frequency ratio increases. These results demonstrate that the proposed controller can provide POD capabilities even when both generators exhibit poorly damped oscillation modes.

VIII. Conclusion

In this paper, a controller based on differential and common power concepts for HVDC interconnections has been introduced. It has been demonstrated that this controller effectively damps low-frequency electro-mechanical oscillations. The introduction of differential and common power concepts shows

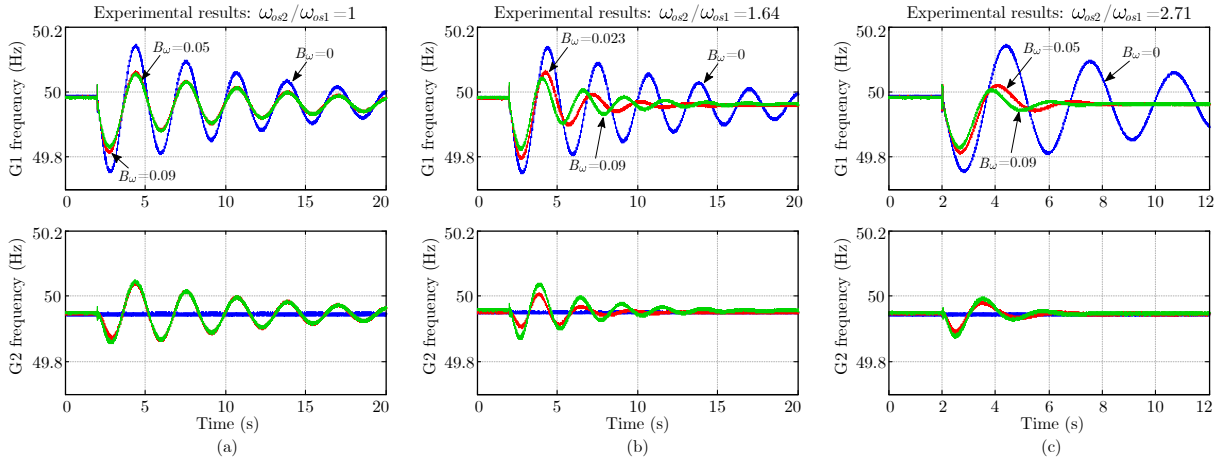

Fig. 16. Experimental results: Transient response of the system when a local load is connected to G1 and generators have a oscillation frequency ratio of (a) $\omega_{os2}/\omega_{os1} = 1$, (b) $\omega_{os2}/\omega_{os1} = 1.64$, and (c) $\omega_{os2}/\omega_{os1} = 2.71$.

clear advantages for the power flow representation of the HVDC connection. The dc-link voltage was used as a measure of the frequency difference between ac grids, avoiding the need for communications. The controller was parametrised so that the equivalent virtual friction represents one of the controller gains, B_ω, providing a clear physical meaning. Moreover, it has been demonstrated that the proposed control scheme is equivalent to a proportional-derivative controller applied to the dc-link voltage. However, an explicit derivative action is not required, making the controller more suitable for power electronics applications.

Both theoretical and experimental results demonstrated that oscillations in two asynchronous grids interconnected by an HVDC link can be effectively damped by using the proposed controller, even when both ac grids have similar inertia and low damping factors. The benefits to system stability from the virtual friction as a novel way to couple two ac networks were demonstrated by utilizing a simple equivalent generator model. Future studies could include further evaluation of the proposed control technique for damping inter-area oscillations explicitly represented in more complex power system models. Other relevant further developments could include the adaptation of the proposed control concept for application in multi-terminal systems, and the evaluation of the performance when implemented for Modular Multilevel Converters (MMCs).

REFERENCES

[1] P. Kundur, N. Balu, and M. Lauby, *Power System Stability and Control*, ser. Discussion Paper Series. McGraw-Hill Education, 1994.

[2] J. P. Sucena-Paiva and L. L. Freris, "Stability of a d.c. transmission link between strong a.c. systems," *Proceedings of the Institution of Electrical Engineers*, vol. 120, no. 10, pp. 1233–1242, October 1973.

[3] J. C. Gonzalez-Torres, V. Costan, G. Damm, A. Benchaib, A. Bertinato, S. Poullain, B. Luscan, and F. Lamnabhi-Lagarrigue, "Hvdc protection criteria for transient stability of ac systems with embedded hvdc links," *The Journal of Engineering*, vol. 2018, pp. 956–960(4), October 2018.

[4] M. A. Elizondo, R. Fan, H. Kirkham, M. Ghosal, F. Wilches-Bernal, D. Schoenwald, and J. Lian, "Interarea oscillation damping control using high-voltage dc transmission: A survey," *IEEE Tran Power Systems*, vol. 33, no. 6, pp. 6915–6923, Nov 2018.

[5] Y. Liu and Z. Chen, "A flexible power control method of vsc-hvdc link for the enhancement of effective short-circuit ratio in a hybrid multi-infeed hvdc system," *IEEE Trans Power Systems*, vol. 28, no. 2, pp. 1568–1581, May 2013.

[6] L. Zeni, R. Eriksson, S. Goumalatsos, M. Altin, P. Srensen, A. Hansen, P. Kjr, and B. Hesselbk, "Power oscillation damping from vschvdc connected offshore wind power plants," *IEEE Tran Power Del*, vol. 31, no. 2, pp. 829–838, April 2016.

[7] H. Latorre and M. Ghandhari, "Improvement of power system stability by using a vsc-hvdc," *International Journal of Electrical Power & Energy Systems*, vol. 33, no. 2, pp. 332 – 339, 2011.

[8] D. Van Hertem, R. Eriksson, L. Sder, and M. Ghandhari, "Coordination of multiple power flow controlling devices in transmission systems," in *9th IET International Conference on AC and DC Power Transmission (ACDC 2010)*, Oct 2010, pp. 1–6.

[9] E. Romero-Ramos, A. Gomez-Exposito, A. Marano-Marcolini, J. M. Maza-Ortega, and J. l. Martinez-Ramos, "Assessing the loadability of active distribution networks in the presence of dc controllable links," *IET Gen, Trans Distri*, vol. 5, no. 11, pp. 1105–1113, Nov 2011.

[10] J. Fang, H. Li, Y. Tang, and F. Blaabjerg, "On the inertia of future more-electronics power systems," *IEEE Journal of Emerging and Selected Topics in Power Electronics*, pp. 1–1, 2018.

[11] X. Liu and A. Lindemann, "Control of vsc-hvdc connected offshore windfarms for providing synthetic inertia," *IEEE Journal of Emerging and Selected Topics in Power Electronics*, vol. 6, no. 3, pp. 1407–1417, Sep. 2018.

[12] R. Aouini, B. Marinescu, K. B. Kilani, and M. Elleuch, "Stability improvement of the interconnection of weak ac zones by synchronverter-based hvdc link," *Electric Power Systems Research*, vol. 142, no. Supplement C, pp. 112–124, 2017.

[13] L. Huang, H. Xin, H. Yang, Z. Wang, and H. Xie, "Interconnecting very weak ac systems by multiterminal vsc-hvdc links with a unified virtual synchronous control," *IEEE Journal of Emerging and Selected Topics in Power Electronics*, vol. 6, no. 3, pp. 1041–1053, Sep. 2018.

[14] Y. Cao, W. Wang, Y. Li, Y. Tan, C. Chen, L. He, U. Hger, and C. Rehtanz, "A virtual synchronous generator control strategy for vsc-mtdc systems," *IEEE Tran Energy Conversion*, vol. 33, no. 2, pp. 750–761, June 2018.

[15] Y. Shen, W. Yao, J. Wen, H. He, and W. Chen, "Adaptive supplementary damping control of vsc-hvdc for interarea oscillation using grhdp," *IEEE Tran Power Systems*, vol. 33, no. 2, pp. 1777–1789, March 2018.

[16] R. Preece, J. V. Milanovi, A. M. Almutairi, and O. Marjanovic, "Damping of inter-area oscillations in mixed ac/dc networks using wams based supplementary controller," *IEEE Tran Power Systems*, vol. 28, no. 2, pp. 1160–1169, May 2013.

[17] B. Pierre, R. Elliott, D. Schoenwald, J. Neely, R. Byrne, D. Trudnowski, and J. Colwell, "Supervisory system for a wide area damping controller using pdci modulation and real-time pmu feedback," in *2016 IEEE Power and Energy Society General Meeting*, 2016, pp. 1–5.

[18] P. Agnihotri, A. Kulkarni, A. M. Gole, B. A. Archer, and T. Weekes, "A robust wide-area measurement-based damping controller for networks with embedded multiterminal and multiinfeed hvdc links," *IEEE Tran Power Systems*, vol. 32, no. 5, pp. 3884–3892, 2017.

[19] Y. Han, H. Li, P. Shen, E. A. A. Coelho, and J. M. Guerrero, "Review of active and reactive power sharing strategies in hierarchical controlled microgrids," *IEEE Tran Power Elec*, vol. 32, no. 3, pp. 2427–2451, March 2017.

[20] Y. Phulpin, "Communication-free inertia and frequency control for wind generators connected by an hvdc-link," *IEEE Tran Power Systems*, vol. 27, no. 2, pp. 1136–1137, May 2012.
[21] J. Rafferty, L. Xu, Y. Wang, G. Xu, and F. Alsokhiry, "Frequency support using multi-terminal hvdc systems based on dc voltage manipulation," *IET Renewable Power Gen*, vol. 10, no. 9, pp. 1393–1401, 2016.
[22] A. E. Leon, "Short-term frequency regulation and inertia emulation using an mmc-based mtdc system," *IEEE Tran Power Systems*, vol. 33, no. 3, pp. 2854–2863, May 2018.
[23] K. Rouzbehi, W. Zhang, J. Ignacio Candela, A. Luna, and P. Rodriguez, "Unified reference controller for flexible primary control and inertia sharing in multi-terminal voltage source converter-hvdc grids," *IET Gen, Tran Distr*, vol. 11, no. 3, pp. 750–758, 2017.
[24] A. Rodríguez-Cabero, J. Roldán-Pérez, M. Prodanovic, J. A. Suul, and S. D'Arco, "Virtual friction control for power system oscillation damping with vsc-hvdc links," in *2019 IEEE Energy Conversion Congress and Exposition (ECCE)*. IEEE, 2019, pp. 1–6.
[25] A. Rodríguez-Cabero, M. Prodanovic, and J. Roldán-Pérez, "Full-state feedback control of back-to-back converters based on differential and common power concepts," *IEEE Tran Ind Elec*, pp. 1–1, 2018.
[26] H. Bevrani, B. François, and T. Ise, *Microgrid Dynamics and Control*. Wiley, 2017.
[27] E. Rakhshani, D. Remon, A. Mir Cantarellas, and P. Rodriguez, "Analysis of derivative control based virtual inertia in multi-area high-voltage direct current interconnected power systems," *IET Gen, Trans Distr*, vol. 10, no. 6, pp. 1458–1469, 2016.
[28] J. Björk, K. H. Johansson, and L. Harnefors, "Fundamental performance limitations in utilizing hvdc to damp interarea modes," *IEEE Transactions on Power Systems*, vol. 34, no. 2, pp. 1095–1104, March 2019.
[29] A. Rodríguez-Cabero, J. Roldán-Pérez, M. Prodanovic, J. A. Suul, and S. D'Arco, "Virtual friction control for oscillation damping with vsc-hvdc links," in *ECCE (submitted)*, 2019.
[30] A. Kirakosyan, E. F. El-Saadany, M. S. E. Moursi, and K. Al Hosani, "DC Voltage Regulation and Frequency Support in Pilot Voltage Droop-Controlled Multiterminal HVdc Systems," *IEEE Trans Power Del*, vol. 33, no. 3, pp. 1153–1164, 2018.
[31] H. Akagi, Y. Kanazawa, and A. Nabae, "Instantaneous reactive power compensators comprising switching devices without energy storage components," *IEEE Tran Ind Appli*, vol. IA-20, no. 3, pp. 625–630, May 1984.
[32] R. G. Lyons, *Understanding Digital Signal Processing*, 1st ed. Boston, MA, USA: Addison-Wesley Longman Publishing Co., Inc., 1996.
[33] A. Yazdani and R. Iravani, *Voltage-Sourced Converters in Power Systems: Modeling, Control, and Applications*. Wiley-IEEE Press, 2010.
[34] M. Prodanovic, A. Rodríguez-Cabero, M. Jiménez-Carrizosa, and J. Roldán-Pérez, "A rapid prototyping environment for dc and ac microgrids: Smart energy integration lab (seil)," in *ICDCM 2017*, June 2017, pp. 421–427.

Alberto Rodríguez-Cabero obtained his degrees in Industrial Technical Engineering and Industrial Engineering specialized in Electronics in 2011 and 2013, respectively, both from Comillas Pontifical University. In 2016, he obtained the Master in Research in Engineering Systems Modelling in the same University. From 2014 to 2015, he worked as control engineer at Institute for Research in Technology (IIT), Comillas Pontifical University, Madrid. Since September 2015 he is working in the Electrical Systems Unit, Institute IMDEA Energy, Madrid. His areas of interest include the design and control of power electronics converters, power quality and micro-grids.

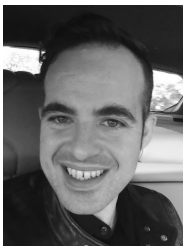

Javier Roldán-Pérez (S'12-M'14) received a B.S. degree in industrial engineering, a M.S. degree in electronics and control systems, a M.S. degree in system modeling, and a Ph.D. degree in power electronics, all from Comillas Pontifical University, Madrid, in 2009, 2010, 2011, and 2015, respectively. From 2010 to 2015, he was with the Institute for Research in Technology (IIT), Comillas University. In 2014, he was a visiting Ph.D. student at the Department of Energy Technology, Aalborg University, Denmark. From 2015 to 2016 he was with the Electric and Control Systems Department at Norvento Energía Distribuida. Currently he is a Senior Assistant Researcher at the Electrical Systems Unit of Institute IMDEA Energy, Madrid, Spain. His research topics are the integration of renewable energies, microgrids, and power electronics applications.

Milan Prodanovic (M'01) received the B.Sc. degree in electrical engineering from the University of Belgrade, Serbia, in 1996 and the Ph.D. degree from Imperial College, London, U.K., in 2004. From 1997 to 1999 he was with GVS engineering company, Serbia, developing UPS systems. From 1999 until 2010 he was a research associate in Electrical and Electronic Engineering at Imperial College, London, UK. Currently he is a Senior Researcher and Head of the Electrical Systems Unit at Institute IMDEA Energy, Madrid, Spain. He authored a number of highly cited articles and is the holder of three patents. His research interests include design and control of power electronics interfaces for distributed generation, micro-grids stability and control and active management of distribution networks.

Jon Are Suul (M'11) received the M.Sc. degree in energy and environmental engineering and the Ph.D. degree in electric power engineering from the Norwegian University of Science and Technology (NTNU), Trondheim, Norway, in 2006 and 2012, respectively. From 2006 to 2007, he was with SINTEF Energy Research, Trondheim, where he was working with simulation of power electronic converters and marine propulsion systems until starting his PhD studies. From 2012, he resumed a position as a Research Scientist at SINTEF Energy Research, first in part-time position while also working as a part-time postdoctoral researcher at the Department of Electric Power Engineering of NTNU until 2016. Since August 2017, he is serving as an Adjunct Associate Professor at the Department of Engineering Cybernetic of NTNU. His research interests are mainly related to modelling, analysis and control of power electronic converters in HVDC transmission, renewable energy applications and electrification of transport.

Salvatore D'Arco received the M.Sc. and Ph.D.degrees in electrical engineering from the University of Naples Federico II, Naples, Italy, in 2002 and 2005, respectively. He was, from 2006 to 2007, a Postdoctoral Researcher with the University of South Carolina, Columbia, SC, USA. In 2008, he joined ASML Holding N.V., Veldhoven, The Netherlands, where he worked as a Power Electronics Designer until 2010. From 2010 to 2012, he was a Postdoctoral Researcher with the Department of Electric Power Engineering, Faculty of Information Technology, Mathematics and Electrical Engineering, Norwegian University of Science and Technology, Trondheim, Norway. In 2012, he joined SINTEF Energy Research, Trondheim, Norway, where he currently works as a Senior Research Scientist. He is the author of over 100 scientific papers, and he is the holder of one patent. His main research activities are related to the control and analysis of power electronic conversion systems for power system applications, including the real-time simulation and rapid prototyping of converter control systems.